

The yielding transition in periodically sheared binary glasses at finite temperature

Nikolai V. Priezjev^{1,2}

¹*Department of Mechanical and Materials Engineering,*

Wright State University, Dayton, OH 45435 and

²*National Research University Higher School of Economics, Moscow 101000, Russia*

(Dated: January 25, 2018)

Abstract

Non-equilibrium molecular dynamics simulations are performed to investigate the dynamic behavior of three-dimensional binary glasses prepared via an instantaneous quench across the glass transition. We found that with increasing strain amplitude up to a critical value, the potential energy approaches lower minima in steady state, whereas the amplitude of shear stress oscillations becomes larger. Below the yielding transition, the storage modulus dominates the mechanical response, and the gradual decay of the potential energy over consecutive cycles is accompanied by reduction in size of transient clusters of atoms with large nonaffine displacements. In contrast, above the yield strain, the loss modulus increases and the system settles at a higher level of potential energy due to formation of a system-spanning shear band after a number of transient cycles.

Keywords: glasses, deformation, temperature, strain amplitude, molecular dynamics simulations

I. INTRODUCTION

The deformation and flow dynamics of yield stress materials, which include foams, gels and glasses, generally depend on physical aging processes, shear-induced rejuvenation, and shear banding, as well as wall slip and finite-size effects [1]. At the microscopic scale, the elementary plastic deformation in disordered materials occurs in a small volume occupied by a group of particles undergoing irreversible rearrangements, sometimes referred to as the shear transformation zone [2–4]. Thus, it was recently shown that during tension-compression cyclic loading of metallic glasses, the initiation of a shear band takes place at the sample surface when aggregates of shear transformation zones reach a critical size [5]. In addition, the results of cyclic nanoindentation tests on metallic glasses have revealed that hardening occurs due to irreversible particle displacements in small volumes beneath the indenter and stiffening of the preferred yielding path [6–10]. Despite significant experimental and computational efforts, the combined effect of microplasticity and confined geometry on the mechanical properties of disordered solids remains not fully understood.

In the last few years, the mechanical response of disordered solids to oscillatory shear deformation was investigated by a number of groups using molecular dynamics simulations [11–24]. It was found that in the elastic range of deformation at zero temperature, particles with large amplitudes of repetitive displacements are organized into clusters [15], while at finite temperatures some trajectories become irreversible [11, 16, 17]. When the thermal fluctuations are not important, the yielding transition is accompanied by a sharp increase of the irreversible particle diffusion, whereas the static structure remains unaffected [18]. Interestingly, it was recently shown for five model glasses that the loss modulus exhibits a characteristic peak in the high-frequency regime that overlaps with the range of natural vibrational frequencies, while at low frequencies, persistent damping arises from long time-scale local, irreversible deformation [23]. Furthermore, cyclic loading with the strain amplitude below (above) the yield point results in the formation of transient clusters (a permanent shear band) of atoms with large nonaffine displacements [19]. With increasing strain amplitude, the thickness of the shear band increases until it becomes comparable to the linear system size [19, 20]. However, the exact mechanism of shear band formation in periodically driven disordered solids has not yet been determined.

In the recent study, the periodic deformation of binary glasses, prepared via instantaneous

quench from a liquid phase to temperatures of about two to six orders of magnitude smaller than the glass transition temperature, was examined using atomistic simulations [24]. In particular, it was shown that the number of cycles required to reach a state with minimum potential energy is larger at higher temperatures and/or larger strain amplitudes. Moreover, the gradual decrease in potential energy was found to correlate with the size of clusters of atoms with large nonaffine displacements. On the other hand, the amplitude of shear stress oscillations in the elastic regime reaches a maximum value when a large part of the system starts to deform reversibly [24].

In this paper, we use non-equilibrium molecular dynamics simulations to study the dynamic response of poorly annealed binary glasses to periodic shear at a temperature approximately one quarter of the glass transition temperature. In agreement with the results of the previous study [24], we find that below the yielding transition, the potential energy gradually decreases to a level that is deeper for larger strain amplitudes. Above the yield strain, the potential energy approaches a higher value, and the amplitude of shear stress oscillations is reduced in the steady state, which is characterized by a system-spanning shear band and enhanced diffusion of particles. It will be shown that the transition from transient clusters to a permanent shear band is reflected in the shape of the probability distribution function of nonaffine displacements.

The remainder of the paper is organized as follows. In the next section, the molecular dynamics simulation method is described. The simulation results for the potential energy, shear stress, mechanical properties, and nonaffine displacements of atoms as a function of the strain amplitude are presented in Sec. III. A brief summary of the results is given in the last section.

II. MOLECULAR DYNAMICS SIMULATIONS

The model glass is represented by the three-dimensional (80:20) binary mixture originally introduced by Kob and Andersen [25] to describe the amorphous metal alloy Ni₈₀P₂₀ [26]. In the Kob-Andersen (KA) model, the interaction between neighboring atoms of types $\alpha, \beta = A, B$ is specified via the truncated Lennard-Jones (LJ) potential:

$$V_{\alpha\beta}(r) = 4\varepsilon_{\alpha\beta} \left[\left(\frac{\sigma_{\alpha\beta}}{r} \right)^{12} - \left(\frac{\sigma_{\alpha\beta}}{r} \right)^6 \right], \quad (1)$$

with the following parametrization $\varepsilon_{AA} = 1.0$, $\varepsilon_{AB} = 1.5$, $\varepsilon_{BB} = 0.5$, $\sigma_{AB} = 0.8$, $\sigma_{BB} = 0.88$, and $m_A = m_B$ [25]. This choice of interaction parameters prevents crystallization below the glass transition temperature [25]. The cutoff radius is fixed $r_{c,\alpha\beta} = 2.5 \sigma_{\alpha\beta}$ to reduce computational cost. All results are reported in the reduced LJ units of length, mass, energy, and time, which are set to $\sigma = \sigma_{AA}$, $m = m_A$, $\varepsilon = \varepsilon_{AA}$, and $\tau = \sigma \sqrt{m/\varepsilon}$, respectively. The integration of the equations of motion was performed using the velocity Verlet algorithm [27] with the time step $\Delta t_{MD} = 0.005 \tau$ [28].

The equilibration was first performed at the high temperature of $1.1 \varepsilon/k_B$, which is well above the critical temperature $T_c \approx 0.435 \varepsilon/k_B$ of the KA model [25]. Here, k_B denotes the Boltzmann constant. All simulations were carried out at a constant volume and the atomic density $\rho = \rho_A + \rho_B = 1.2 \sigma^{-3}$. The total number of atoms is $N = 60\,000$ and the linear size of the periodic cubic cell is $L = 36.84 \sigma$. Next, following an instantaneous quench across the glass transition to the temperature $T_{LJ} = 0.1 \varepsilon/k_B$, the system was subjected to time periodic shear deformation as follows:

$$\gamma(t) = \gamma_0 \sin(2\pi t/T), \quad (2)$$

where γ_0 is the strain amplitude and T is the period of oscillation. The shear deformation was applied parallel to the xz plane (see Fig. 1) by using the Lees-Edwards periodic boundary conditions and the SLLOD algorithm [29]. In addition, the temperature $T_{LJ} = 0.1 \varepsilon/k_B$ was maintained by the dissipative particle dynamics (DPD) thermostat, which ensures that the particle dynamics is not coupled to the imposed flow profile [30]. In the present study, the oscillation period was fixed to $T = 5000 \tau$ and the strain amplitude was varied in the range $0.03 \leq \gamma_0 \leq 0.07$. The data for the shear stress, potential energy, and atom positions were collected during 600 shear cycles for each value of the strain amplitude. The postprocessing analysis was performed only in one sample due to computational restrictions.

III. RESULTS

The structure and properties of metallic glasses depend strongly on the details of the production and processing routes [31]. For example, it is well known that upon slower cooling, the glassy system can reach states with lower potential energy and smaller volume [31]. Moreover, under applied deformation, the system can further explore different regions of the

potential energy landscape that are hardly accessible otherwise [32]. Thus, it was demonstrated that one shear cycle with large strain amplitude rejuvenates the glass by moving it to a state with shallower energy minima, whereas one small-strain cycle overages the glass by reaching a state with deeper energy minima [32]. Furthermore, it was recently shown that with increasing cooling rate, the strain-induced energy loss per strain (caused by particle rearrangements) increases and glasses become more ductile and less reversible [21]. In the present study, the binary mixture in a high-temperature liquid state is instantaneously quenched across the glass transition and then subjected to periodic deformation for hundreds of cycles with strain amplitudes above and below the yielding transition.

The variation of the potential energy, U/ε , during 600 shear cycles after the thermal quench to $T_{LJ} = 0.1 \varepsilon/k_B$ is shown in Fig. 2 for the strain amplitudes $\gamma_0 = 0.03, 0.04, 0.05, 0.06$ and 0.07 . Note that the data for all strain amplitudes except for $\gamma_0 = 0.05$ are displaced vertically for clarity (see caption to Fig. 2). It can be clearly seen that the potential energy decreases rapidly during the first few tens of shear cycles and then it gradually saturates to a nearly constant value for each strain amplitude. In the case $\gamma_0 = 0.06$, however, a markedly different behavior is observed; namely, the local minimum is developed at $t \approx 80 T$ (see Fig. 2). In other words, the system is first driven to a relatively deep energy minimum, where the amplitude of energy oscillations is enhanced, followed by a crossover to a steady state with a higher potential energy and reduced energy amplitude. For all cases presented in Fig. 2, the steady state with the lowest potential energy, $U \approx -8.16 \varepsilon$, is achieved at $\gamma_0 = 0.05$, which suggests that the critical strain amplitude for the yielding transition is in the range between 0.05 and 0.06 at the temperature $T_{LJ} = 0.1 \varepsilon/k_B$. For comparison, the cyclic loading with $\gamma_0 = 0.05$ at lower temperatures, $T_{LJ} \leq 10^{-2} \varepsilon/k_B$, resulted in the states with the potential energy $U \approx -8.26 \varepsilon$, and the critical strain amplitude was found to be greater than 0.07 [24]. We also comment that the potential energy saturates at $U \approx -8.12 \varepsilon$ when the system is instantaneously quenched to $T_{LJ} = 0.1 \varepsilon/k_B$ and evolves in the absence of periodic shear.

The time dependence of the shear stress during 600 cycles is illustrated in Fig. 3 for the same strain amplitudes $\gamma_0 = 0.03, 0.04, 0.05, 0.06$ and 0.07 as in Fig. 2. Notice that the mean value of shear stress is zero but the data for different strain amplitudes in Fig. 3 are displaced upward for visualization. It can be observed that the amplitude of stress

oscillations in steady state increases when the strain amplitude is varied from $\gamma_0 = 0.03$ to 0.05. In the case $\gamma_0 = 0.06$, the stress amplitude during the first 100 cycles becomes even larger than for $\gamma_0 = 0.05$ but upon approaching steady state, $t \gtrsim 200 T$, the shear stress is reduced, indicating significant plastic deformation in the material (discussed below). This behavior is consistent with the appearance of a shallow minimum in the potential energy for the strain amplitude $\gamma_0 = 0.06$ reported in Fig. 2. Finally, the transient regime to steady state is reduced to only a few cycles for the strain amplitude $\gamma_0 = 0.07$, and the stress amplitudes become nearly the same for the cases $\gamma_0 = 0.06$ and 0.07 when $t \gtrsim 200 T$.

We next plot the storage (G') and loss (G'') moduli as a function of the strain amplitude in Fig. 4. The data were computed from the shear stress curves, $\sigma_{xz}(t)$, in steady state using the definitions $G' = \sigma_{xz}^{max}/\gamma_0 \cos(\delta)$ and $G'' = \sigma_{xz}^{max}/\gamma_0 \sin(\delta)$, where δ is the phase difference between stress and strain [33]. As is evident, the storage modulus is much larger than the loss modulus at small strain amplitudes, $\gamma_0 \leq 0.05$. With further increasing strain amplitude, $\gamma_0 \geq 0.06$, the difference between the storage and loss moduli significantly decreases, indicating the onset of energy dissipation due to plastic deformation. Along with the mechanical properties, we present the mean square displacement of atoms for different strain amplitudes in the inset to Fig. 4. It is clearly seen that a transition between nearly reversible dynamics and diffusive behavior occurs at the strain amplitude $\gamma_0 = 0.06$. These results are consistent with conclusions of the previous study of jammed solids subjected to large-amplitude oscillatory shear, where it was demonstrated that the critical strain amplitude associated with the onset of particle diffusion is smaller than the strain amplitude at which a crossing of G' and G'' occurs [18]. We finally comment that a more gradual increase of the mean square displacement curve at the strain amplitude $\gamma_0 = 0.06$ reported in the previous study [11] is due to much smaller oscillation period $T \approx 314 \tau$ rather than $T = 5000 \tau$ used in the present study.

A complementary analysis of atomic rearrangements during oscillatory shear deformation involves the so-called nonaffine displacements of atoms, which are defined as a deviation from a local linear transformation [4]. In practice, the nonaffine measure can be estimated numerically using the transformation matrix \mathbf{J}_i , which maps all vectors between the i -th

atom and its neighbors during the time interval Δt as follows:

$$D^2(t, \Delta t) = \frac{1}{N_i} \sum_{j=1}^{N_i} \left\{ \mathbf{r}_j(t + \Delta t) - \mathbf{r}_i(t + \Delta t) - \mathbf{J}_i [\mathbf{r}_j(t) - \mathbf{r}_i(t)] \right\}^2, \quad (3)$$

where the sum is carried over the neighbors within the cutoff distance of 1.5σ from $\mathbf{r}_i(t)$. It was recently demonstrated that in periodically sheared glasses, a large fraction of atoms undergo repetitive nonaffine displacements with amplitudes that are broadly distributed [16, 17]. Above the yield strain, some atoms in well-annealed (slowly quenched) binary glasses start to rearrange irreversibly, and, after a number of transient shear cycles, the atoms with large nonaffine displacements were shown to organize into a system-spanning shear band, whose thickness increases at larger strain amplitudes [19].

Spatial configurations of atoms with large nonaffine displacements are displayed in Figs. 5, 6, 7, and 8 for the strain amplitudes $\gamma_0 = 0.03, 0.05, 0.06$ and 0.07 , respectively. It can be seen in Figs. 5 and 6 that at small strain amplitudes, $\gamma_0 \leq 0.05$, the atoms with $D^2 > 0.04\sigma^2$ form relatively large clusters during 20-th cycle, and upon further annealing, the number of atoms with nearly reversible trajectories increases. This behavior is consistent with the gradual decay of the potential energy reported in Fig. 2 and large values of the storage modulus in Fig. 4 for $\gamma_0 \leq 0.05$. In sharp contrast, at large strain amplitudes, $\gamma_0 \geq 0.06$, most of the atoms initially undergo large ($D^2 > 0.04\sigma^2$) nonaffine displacements, and, after a number of transient shear cycles, a system-spanning shear band is formed (see Figs. 7 and 8). Notice that in both cases, $\gamma_0 = 0.06$ and 0.07 , the location of the shear band is displaced along the \hat{z} direction over consecutive cycles. The appearance of the shear band at large strain amplitudes correlates well with the onset of dissipation (larger loss modulus) and enhanced diffusion reported in Fig. 4. We further remark that cycling loading of poorly annealed glasses at lower temperatures, $T_{LJ} \leq 10^{-2} \varepsilon/k_B$, during 600 shear cycles did not result in the formation of shear bands for the strain amplitudes $0.03 \leq \gamma_0 \leq 0.07$ [24].

The observed sequence of patterns (shear bands vs. disconnected clusters) of atoms with large nonaffine displacements is reflected in the shape of probability distribution functions of the nonaffine measure. Next, the probability distribution function of $D^2(t, T)$, averaged within narrow time intervals, are presented in Fig. 9 for the strain amplitudes $\gamma_0 = 0.03, 0.05, 0.06$ and 0.07 . In agreement with the previous studies [16, 17, 19, 34], the nonaffine displacements for all strain amplitudes and time intervals are broadly distributed (see Fig. 9).

However, the time dependence of the probability distributions is markedly different for $\gamma_0 \leq 0.05$ and $\gamma_0 \geq 0.06$. In particular, the shape of the probability distributions for $\gamma_0 = 0.03$ and 0.05 in Fig. 9 (a, b) becomes more narrow over consecutive cycles, indicating progressively more reversible dynamics; while for $\gamma_0 = 0.07$ shown in Fig. 9 (d), the opposite trend emerges. The most peculiar case is shown for the strain amplitude $\gamma_0 = 0.06$ in Fig. 9 (c), where the distribution of D^2 first becomes more narrow and then slightly broadens as the number of cycles increases. This behavior is correlated with the nonmonotonic transient of the potential energy shown in Fig. 2 and the temporary increase of the shear stress oscillations in Fig. 3. Overall, we conclude that at the higher target temperature $T_{LJ} = 0.1 \varepsilon/k_B$ (in comparison with the range $10^{-6} \varepsilon/k_B \leq T_{LJ} \leq 10^{-2} \varepsilon/k_B$ considered in the previous study [24]), the critical strain amplitude of the yielding transition is decreased below $\gamma_0 = 0.06$. We finally comment that a decrease in storage modulus and proliferation of large nonaffine particle displacements at the strain amplitude $\gamma_0 = 0.06$ might be related to the onset of yielding formulated in terms of loss of long-lived nearest neighbors [35].

IV. CONCLUSIONS

In summary, non-equilibrium molecular dynamics simulations were performed to examine the dynamic response of a three-dimensional model glass to oscillatory shear deformation. The model glass was represented by a binary Lennard-Jones mixture that was rapidly quenched from a high-temperature liquid state to a temperature of about a quarter of the glass transition temperature. Following the thermal quench, the binary glass was subjected to periodic shear at constant volume over hundreds of cycles. To ensure that particle dynamics is not coupled to the imposed flow profile, the dissipative particle dynamics thermostat was applied during periodic shear deformation.

It was shown that with increasing strain amplitude up to a critical value, the potential energy acquires progressively lower minima, while the amplitude of stress oscillations in steady state becomes larger. Moreover, the gradual decay of the potential energy is associated with sparse clusters of atoms with large nonaffine displacements. Above the yielding transition, the viscoelastic damping increases and the potential energy in steady state becomes higher. The initial stage of the structural relaxation process involves transient clusters of atoms with large nonaffine displacements, followed by the formation of a permanent shear band that

runs across the whole system. Upon cyclic loading, the width of the probability distribution function of nonaffine displacements increases (decreases) for strain amplitudes above (below) the yielding transition.

Acknowledgments

Financial support from the National Science Foundation (CNS-1531923) is gratefully acknowledged. The article was prepared within the framework of the Basic Research Program at the National Research University Higher School of Economics (HSE) and supported within the framework of a subsidy by the Russian Academic Excellence Project ‘5-100’. The molecular dynamics simulations were performed using the LAMMPS numerical code developed at Sandia National Laboratories [28]. Computational work in support of this research was performed at Michigan State University’s High Performance Computing Facility and the Ohio Supercomputer Center.

-
- [1] D. Bonn, M. M. Denn, L. Berthier, T. Divoux, and S. Manneville, Yield stress materials in soft condensed matter, *Rev. Mod. Phys.* **89**, 035005 (2017).
 - [2] A. S. Argon, Plastic deformation in metallic glasses, *Acta Metall.* **27**, 47 (1979).
 - [3] F. Spaepen, A microscopic mechanism for steady state inhomogeneous flow in metallic glasses, *Acta Metall.* **25**, 407 (1977).
 - [4] M. L. Falk and J. S. Langer, Dynamics of viscoplastic deformation in amorphous solids, *Phys. Rev. E* **57**, 7192 (1998).
 - [5] Z. D. Sha, S. X. Qu, Z. S. Liu, T. J. Wang, and H. Gao, Cyclic deformation in metallic glasses, *Nano Lett.* **15**, 7010 (2015).
 - [6] C. E. Packard, L. M. Witmer, and C. A. Schuh, Hardening of a metallic glass during cyclic loading in the elastic range, *Appl. Phys. Lett.* **92**, 171911 (2008).
 - [7] C. Deng and C. A. Schuh, Atomistic mechanisms of cyclic hardening in metallic glass, *Appl. Phys. Lett.* **100**, 251909 (2012).
 - [8] N. Wang, F. Yan, and L. Li, Mesoscopic examination of cyclic hardening in metallic glass, *J. Non-Cryst. Solids* **428**, 146 (2015).

- [9] D. Zhao, H. Zhao, B. Zhu, and S. Wang, Investigation on hardening behavior of metallic glass under cyclic indentation loading via molecular dynamics simulation, *Appl. Surf. Sci.* **416**, 14 (2017).
- [10] H. R. Lashgari, C. Tang, D. Chu, and S. Li, Molecular dynamics simulation of cyclic indentation in Fe-based amorphous alloy, *Comput. Mater. Sci.* **143**, 473 (2018).
- [11] N. V. Priezjev, Heterogeneous relaxation dynamics in amorphous materials under cyclic loading, *Phys. Rev. E* **87**, 052302 (2013).
- [12] D. Fiocco, G. Foffi, and S. Sastry, Oscillatory athermal quasistatic deformation of a model glass, *Phys. Rev. E* **88**, 020301(R) (2013).
- [13] I. Regev, T. Lookman, and C. Reichhardt, Onset of irreversibility and chaos in amorphous solids under periodic shear, *Phys. Rev. E* **88**, 062401 (2013).
- [14] N. V. Priezjev, Dynamical heterogeneity in periodically deformed polymer glasses, *Phys. Rev. E* **89**, 012601 (2014).
- [15] I. Regev, J. Weber, C. Reichhardt, K. A. Dahmen, and T. Lookman, Reversibility and criticality in amorphous solids, *Nat. Commun.* **6**, 8805 (2015).
- [16] N. V. Priezjev, Reversible plastic events during oscillatory deformation of amorphous solids, *Phys. Rev. E* **93**, 013001 (2016).
- [17] N. V. Priezjev, Nonaffine rearrangements of atoms in deformed and quiescent binary glasses, *Phys. Rev. E* **94**, 023004 (2016).
- [18] T. Kawasaki and L. Berthier, Macroscopic yielding in jammed solids is accompanied by a non-equilibrium first-order transition in particle trajectories, *Phys. Rev. E* **94**, 022615 (2016).
- [19] N. V. Priezjev, Collective nonaffine displacements in amorphous materials during large-amplitude oscillatory shear, *Phys. Rev. E* **95**, 023002 (2017).
- [20] P. Leishangthem, A. D. S. Parmar, and S. Sastry, The yielding transition in amorphous solids under oscillatory shear deformation, *Nat. Commun.* **8**, 14653 (2017).
- [21] M. Fan, M. Wang, K. Zhang, Y. Liu, J. Schroers, M. D. Shattuck, and C. S. O'Hern, The effects of cooling rate on particle rearrangement statistics: Rapidly cooled glasses are more ductile and less reversible, *Phys. Rev. E* **95**, 022611 (2017).
- [22] S. Dagois-Bohy, E. Somfai, B. P. Tighe, and M. van Hecke, Softening and yielding of soft glassy materials, *Soft Matter* **13**, 9036 (2017).
- [23] R. Ranganathan, Y. Shi, and P. Koblinski, Commonalities in frequency-dependent viscoelastic

- damping in glasses in the MHz to THz regime, *J. Appl. Phys.* **122**, 145103 (2017).
- [24] N. V. Priezjev, Molecular dynamics simulations of the mechanical annealing process in metallic glasses: Effects of strain amplitude and temperature, *J. Non-Cryst. Solids* **479**, 42 (2018).
- [25] W. Kob and H. C. Andersen, Testing mode-coupling theory for a supercooled binary Lennard-Jones mixture: The van Hove correlation function, *Phys. Rev. E* **51**, 4626 (1995).
- [26] T. A. Weber and F. H. Stillinger, Local order and structural transitions in amorphous metal-metalloid alloys, *Phys. Rev. B* **31**, 1954 (1985).
- [27] M. P. Allen and D. J. Tildesley, *Computer Simulation of Liquids* (Clarendon, Oxford, 1987).
- [28] S. J. Plimpton, Fast parallel algorithms for short-range molecular dynamics, *J. Comp. Phys.* **117**, 1 (1995).
- [29] D. J. Evans and G. P. Morriss, *Statistical Mechanics of Nonequilibrium Liquids* (Academic Press, London, 1990).
- [30] T. Soddemann, B. Dunweg, and K. Kremer, Dissipative particle dynamics: A useful thermostat for equilibrium and nonequilibrium molecular dynamics simulations, *Phys. Rev. E* **68**, 046702 (2003).
- [31] Y. Sun, A. Concustell, and A. L. Greer, Thermomechanical processing of metallic glasses: extending the range of the glassy state, *Nat. Rev. Mater.* **1**, 16039 (2016).
- [32] D. J. Lacks and M. J. Osborne, Energy landscape picture of overaging and rejuvenation in a sheared glass, *Phys. Rev. Lett.* **93**, 255501 (2004).
- [33] K. Hyun, M. Wilhelm, C. O. Klein, K. S. Cho, J. G. Nam, K. H. Ahn, S. J. Lee, R. H. Ewoldt, and G. H. McKinley, A review of nonlinear oscillatory shear tests: Analysis and application of large amplitude oscillatory shear (LAOS), *Prog. Polym. Sci.* **36**, 1697 (2011).
- [34] V. Chikkadi and P. Schall, Nonaffine measures of particle displacements in sheared colloidal glasses, *Phys. Rev. E* **85**, 031402 (2012).
- [35] L. Perez-Ocampo, A. Zaccone, and M. Laurati, A well defined glass state obtained by oscillatory shear, *Journal of Rheology* **62**, 197 (2018).

Figures

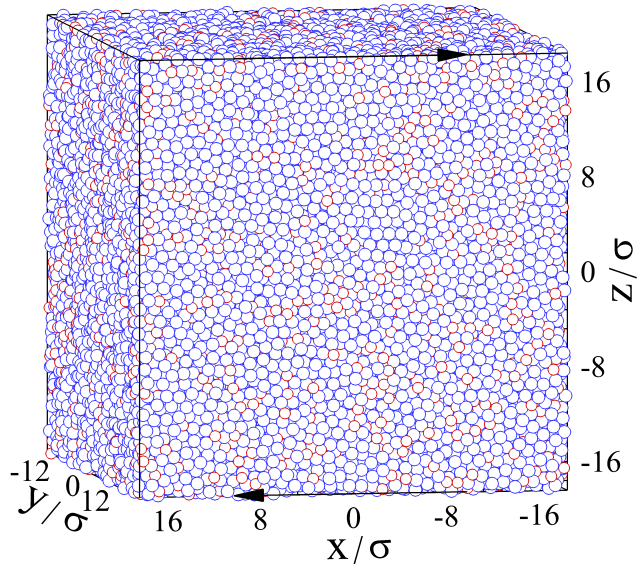


FIG. 1: (Color online) A snapshot of the annealed Lennard-Jones binary glass after 600 shear cycles with the strain amplitude $\gamma_0 = 0.05$. The temperature is $T_{LJ} = 0.1 \varepsilon/k_B$ and the oscillation period is $T = 5000 \tau$. The plane of shear is denoted by black arrows. Atoms of types A and B (blue and red circles) are now drawn to scale.

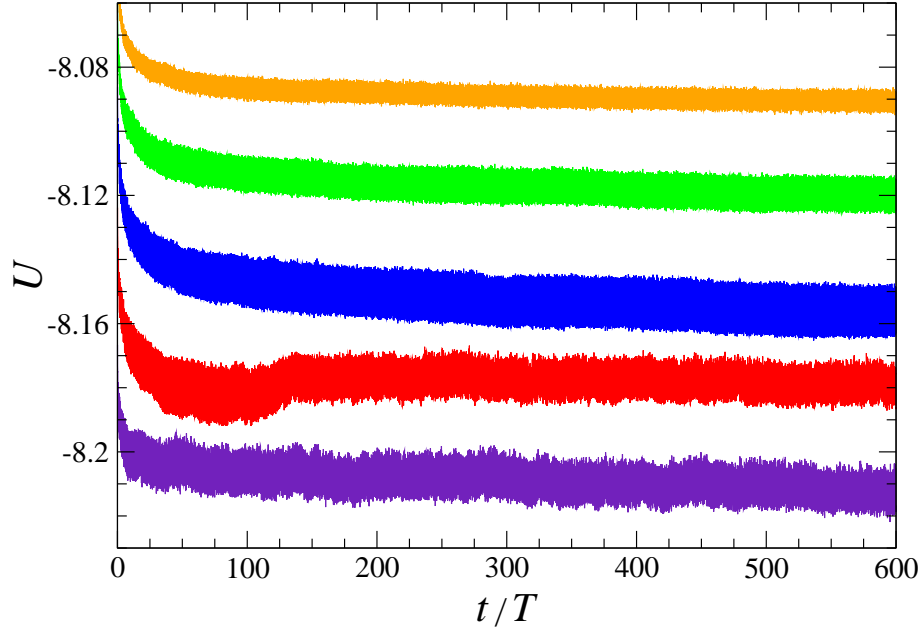


FIG. 2: (Color online) The time dependence of the potential energy per particle U (in units of ε) during 600 shear cycles for the strain amplitudes $\gamma_0 = 0.03$ (orange), 0.04 (green), 0.05 (blue), 0.06 (red), and 0.07 (indigo). For clarity, the data were displaced vertically by $+0.05\varepsilon$ for $\gamma_0 = 0.03$, by $+0.03\varepsilon$ for $\gamma_0 = 0.04$, by -0.04ε for $\gamma_0 = 0.06$, and by -0.08ε for $\gamma_0 = 0.07$. The data for $\gamma_0 = 0.05$ were left as is. The oscillation period is $T = 5000\tau$ and the temperature is $T_{LJ} = 0.1\varepsilon/k_B$.

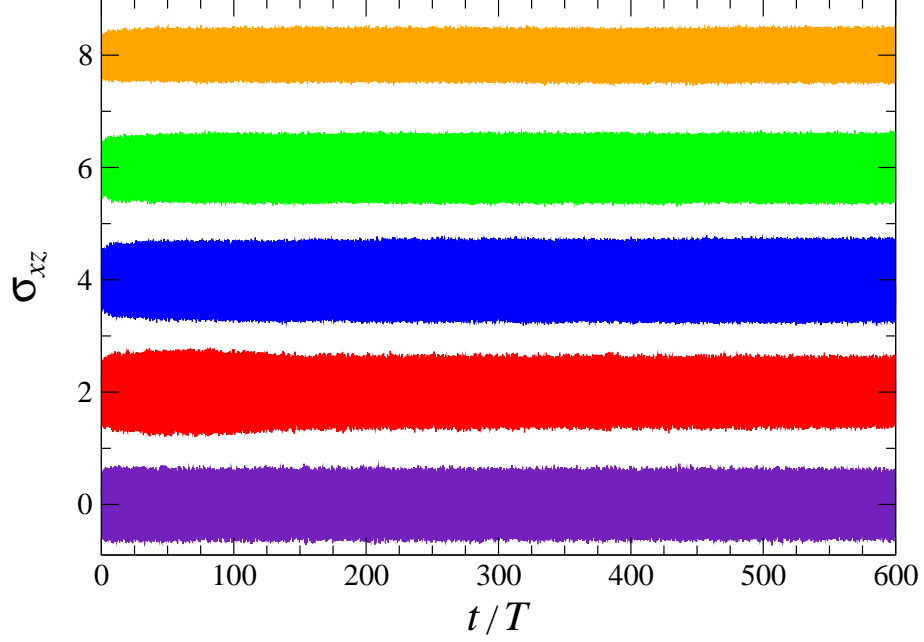


FIG. 3: (Color online) The variation of the shear stress σ_{xz} (in units of $\varepsilon\sigma^{-3}$) for the strain amplitudes $\gamma_0 = 0.03$ (orange), 0.04 (green), 0.05 (blue), 0.06 (red), and 0.07 (indigo). The data were displaced by $8.0\varepsilon\sigma^{-3}$ for $\gamma_0 = 0.03$, by $6.0\varepsilon\sigma^{-3}$ for $\gamma_0 = 0.04$, by $4.0\varepsilon\sigma^{-3}$ for $\gamma_0 = 0.05$, and by $2.0\varepsilon\sigma^{-3}$ for $\gamma_0 = 0.06$. The period of oscillation is $T = 5000\tau$.

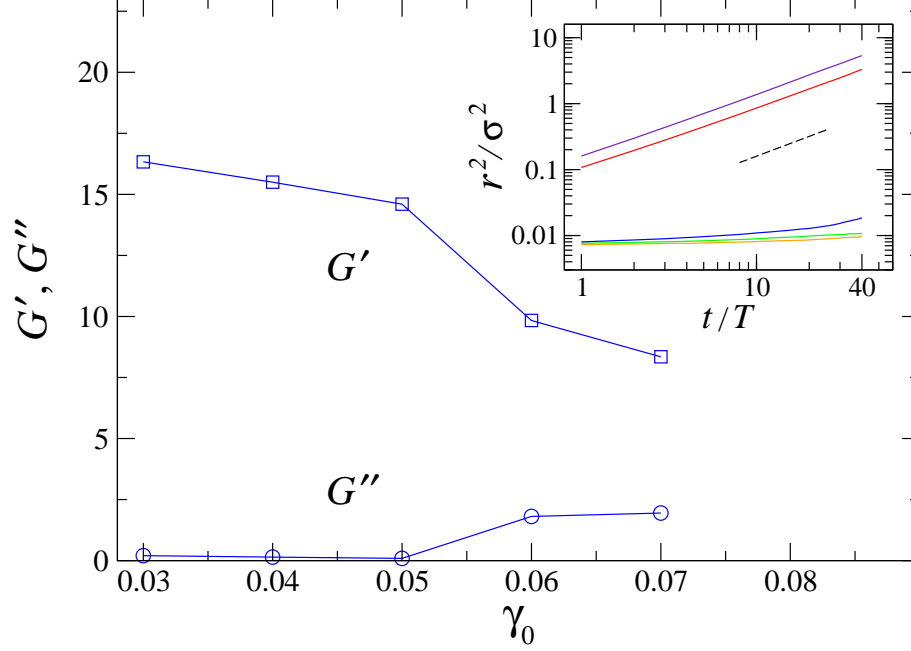


FIG. 4: (Color online) The storage (G') and loss (G'') moduli (in units of $\varepsilon\sigma^{-3}$) as a function of the strain amplitude. The inset shows the mean square displacement of atoms for the strain amplitudes $\gamma_0 = 0.03$ (orange), 0.04 (green), 0.05 (blue), 0.06 (red), and 0.07 (indigo). The data were averaged over the last 40 shear cycles. The straight dashed line indicates the unit slope.

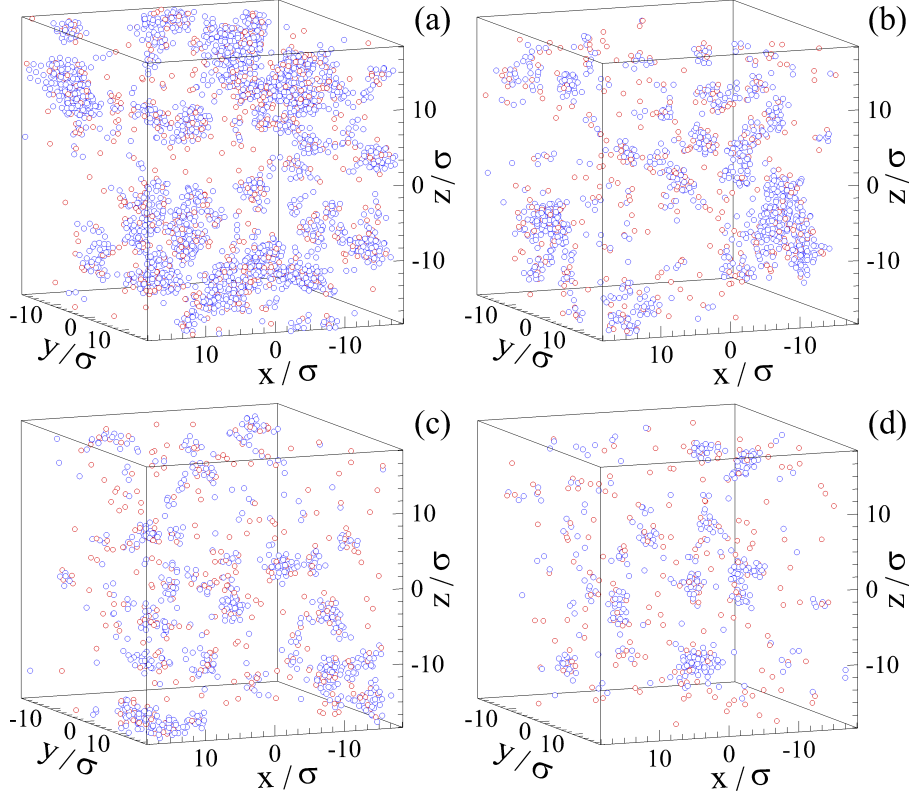


FIG. 5: (Color online) Snapshots of atomic configurations for the strain amplitude $\gamma_0 = 0.03$, temperature $T_{LJ} = 0.1 \varepsilon/k_B$, and nonaffine measure (a) $D^2(19T, T) > 0.04 \sigma^2$, (b) $D^2(79T, T) > 0.04 \sigma^2$, (c) $D^2(199T, T) > 0.04 \sigma^2$, and (d) $D^2(599T, T) > 0.04 \sigma^2$.

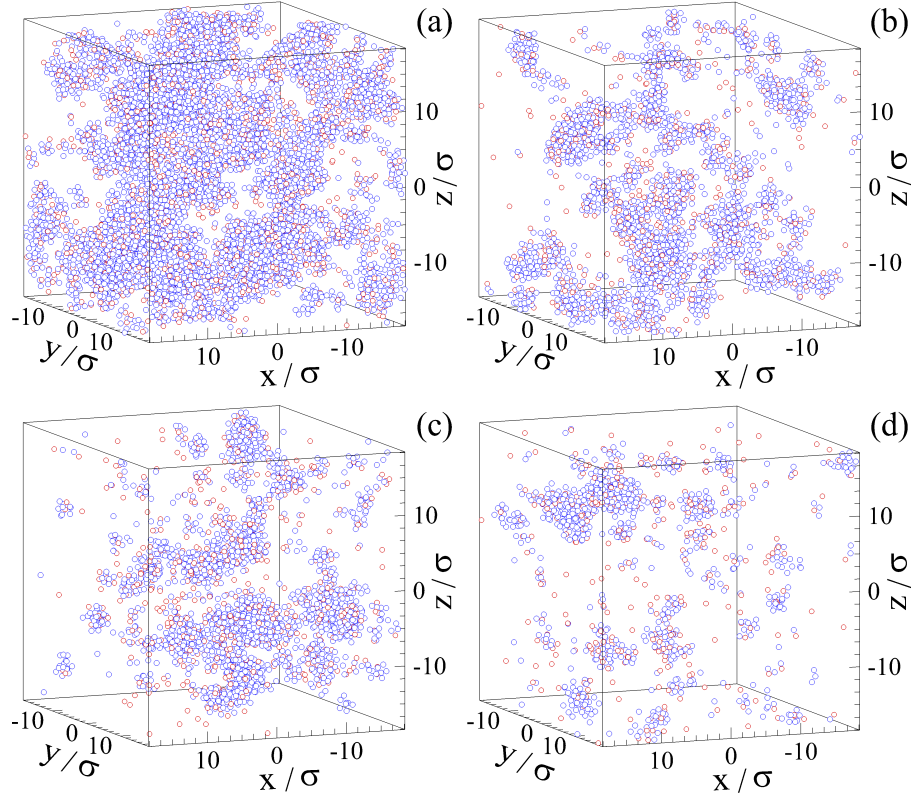


FIG. 6: (Color online) Spatial configurations of atoms with large nonaffine displacements (a) $D^2(19T, T) > 0.04 \sigma^2$, (b) $D^2(79T, T) > 0.04 \sigma^2$, (c) $D^2(199T, T) > 0.04 \sigma^2$, and (d) $D^2(599T, T) > 0.04 \sigma^2$. The strain amplitude is $\gamma_0 = 0.05$ and temperature is $T_{LJ} = 0.1 \epsilon/k_B$.

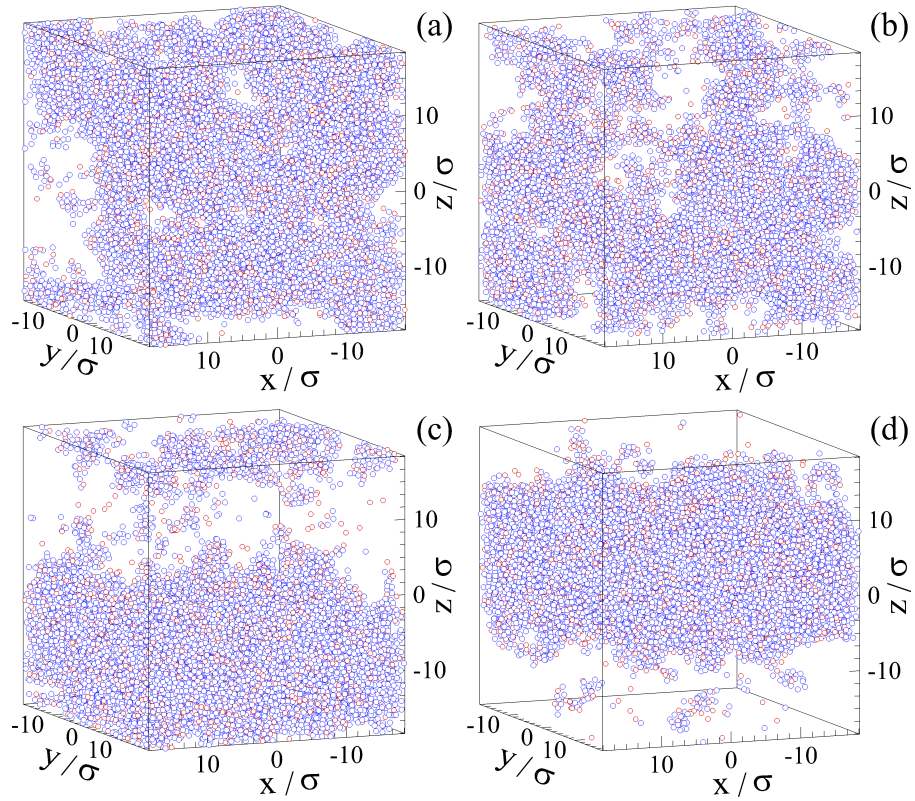


FIG. 7: (Color online) Atomic positions for the strain amplitude $\gamma_0 = 0.06$, temperature $T_{LJ} = 0.1\varepsilon/k_B$, and nonaffine measure (a) $D^2(19T, T) > 0.04\sigma^2$, (b) $D^2(79T, T) > 0.04\sigma^2$, (c) $D^2(199T, T) > 0.04\sigma^2$, and (d) $D^2(599T, T) > 0.04\sigma^2$.

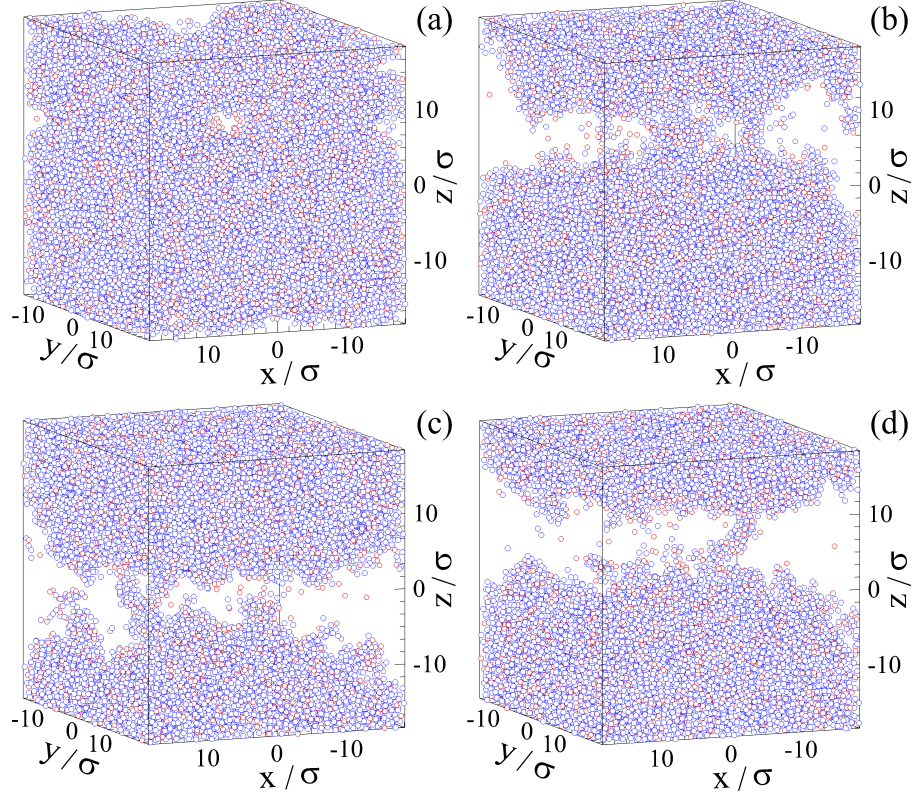


FIG. 8: (Color online) Snapshots of atomic positions for the strain amplitude $\gamma_0 = 0.07$ and nonaffine measure (a) $D^2(19T, T) > 0.04\sigma^2$, (b) $D^2(79T, T) > 0.04\sigma^2$, (c) $D^2(199T, T) > 0.04\sigma^2$, and (d) $D^2(599T, T) > 0.04\sigma^2$. The temperature of the system is $T_{LJ} = 0.1\epsilon/k_B$.

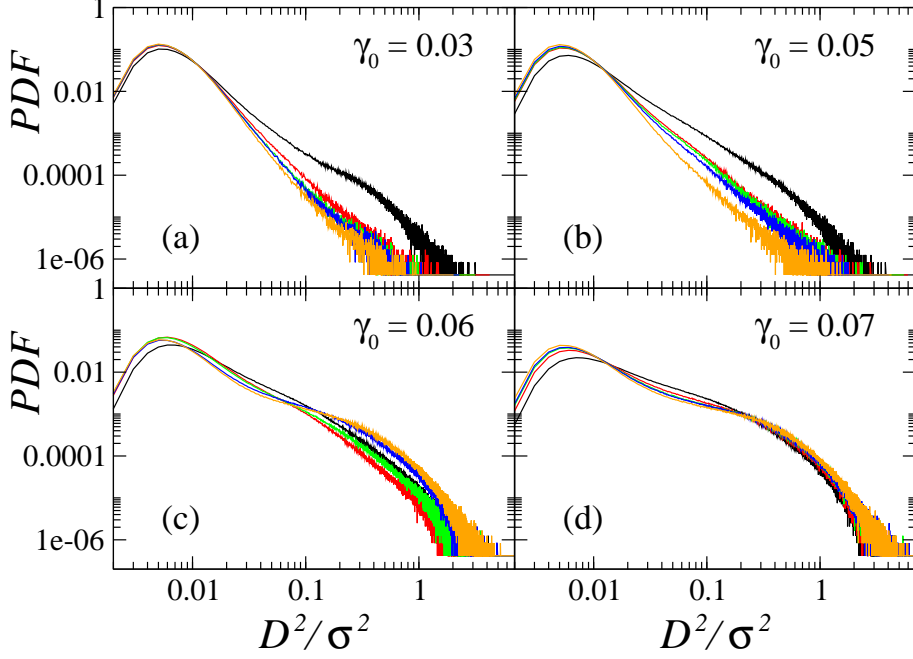


FIG. 9: (Color online) The normalized probability distribution functions of the nonaffine measure $D^2(t, T)$ for the strain amplitudes (a) $\gamma_0 = 0.03$, (b) $\gamma_0 = 0.05$, (c) $\gamma_0 = 0.06$, and (d) $\gamma_0 = 0.07$. The data are averaged during the following time intervals $0 \leq t \leq 40T$ (black curves), $40T \leq t \leq 80T$ (red curves), $80T \leq t \leq 120T$ (green curves), $160T \leq t \leq 200T$ (blue curves), and $560T \leq t \leq 600T$ (orange curves).